Petroleum Science 19 (2022) 203–210

Contents lists available at ScienceDirect

Petroleum Science

journal homepage: www.keaipublishing.com/en/journals/petroleum-science

Original Paper

Effect of confinement on the three-phase equilibrium of water-oil-CO_2 mixtures in nanopores

Yi-Lei Song [a], Shao-Hua Gu [b], Zhao-Jie Song [a, *], Zhuo-Ya Zhang [a], Xu-Ya Chang [a], Jia Guo [a]

[a] State Key Laboratory of Petroleum Resources and Prospecting and Unconventional Petroleum Research Institute, China University of Petroleum-Beijing, Beijing, 102249, China
[b] Sinopec Petroleum Exploration and Production Research Institute, Beijing, 100083, China

ARTICLE INFO

Article history:
Received 5 May 2021
Accepted 13 August 2021
Available online 17 September 2021

Edited by Yan-Hua Sun

Keywords:
Three-phase behavior
Water-oil-CO_2 mixtures
Nanopore confinement
CO_2 enhanced oil recovery
Shale reservoirs

ABSTRACT

Accurate characterization of fluid phase behavior is an important aspect of CO_2 enhanced shale oil recovery. So far, however, there has been little discussion about the nanopore confinement effect, including adsorption and capillarity on the phase equilibrium of water-oil-CO_2 mixtures. In this study, an improved three-phase flash algorithm is proposed for calculating the phase behavior of water-oil-gas mixture on the basis of an extended Young-Laplace equation and a newly developed fugacity calculation model. The fugacity model can consider the effect of water-oil-gas adsorption on phase equilibrium. A water-Bakken oil-CO_2 mixture is utilized to verify the accuracy of the flash algorithm and investigate the confinement effect. Results show that the confinement effect promotes the transfer of all components in the vapor phase to other phases, while the transfer of water, CO_2, and lighter hydrocarbons is more significant. This leads to a large decrease, a large increase, and a small increase in the mole fraction of the vapor, oleic, and aqueous phases, respectively. When the confinement effect is considered, the density difference of vapor-oleic phases decreases, and the interfacial tension of vapor-oleic phases decreases; however, the density difference of vapor-aqueous phases increases, the interfacial tension of vapor-aqueous phases still decreases.

1. Introduction

Shale oil plays an increasingly significant role in the energy industry and is expected to become a major contributor to the continued growth of crude production worldwide. The reserves of global shale oil resources are considerable, reaching 67,840 × 10^8 barrels (Song et al., 2020c). The development of technologies such as hydraulic fracturing and horizontal wells has led to the successful production of shale oil, but the oil recovery from shale formations is still unsatisfactory. Recently, the use of CO_2 as an injection agent to further improve shale oil recovery has attracted more and more attention (Wu et al., 2020; Zhu et al., 2021). However, the addition of CO_2 causes the interphase mass transfers and thermodynamic properties of formation fluids to be very complicated (Zhou et al., 2020). To date, the knowledge of the phase behavior of formation fluids considering the CO_2 addition in shale reserves is still insufficient, which brings difficulties to the optimization design of the shale oil production (Song et al., 2021a). Hence, more research needs to be carried out to increase our knowledge of the phase behavior of shale fluids after CO_2 injection.

The pore-throats of shale reservoirs are on the nanometer scale (Li and Sheng, 2017). For example, in the Bakken reservoir, the radius of pore-throat is mostly between 1 and 40 nm (Nojabaei et al., 2013). The small pore size in shale formation creates spatial confinement, which leads to the unpredictable phase behavior of shale fluids (Feng et al., 2021; Yang et al., 2019). The nanopore confinement effect in shale reservoirs changes the phase behavior due to two main reasons: high capillary force (Zhang et al., 2017) and strong fluid adsorption (Song et al., 2020b). Fluid adsorption causes changes in pore size and wettability, thereby enhancing the capillarity. Besides, the fluid adsorption in nanopores may change the composition distribution of the reservoir fluids, thereby having a greater impact on the fluid property and phase behavior (Liu et al., 2018). Understanding the effect of nanopore confinement will help to accurately describe the phase behavior of confined fluids in shale

* Corresponding author.
E-mail addresses: songyilei25@163.com (Y.-L. Song), songz@cup.edu.cn (Z.-J. Song).

https://doi.org/10.1016/j.petsci.2021.09.024

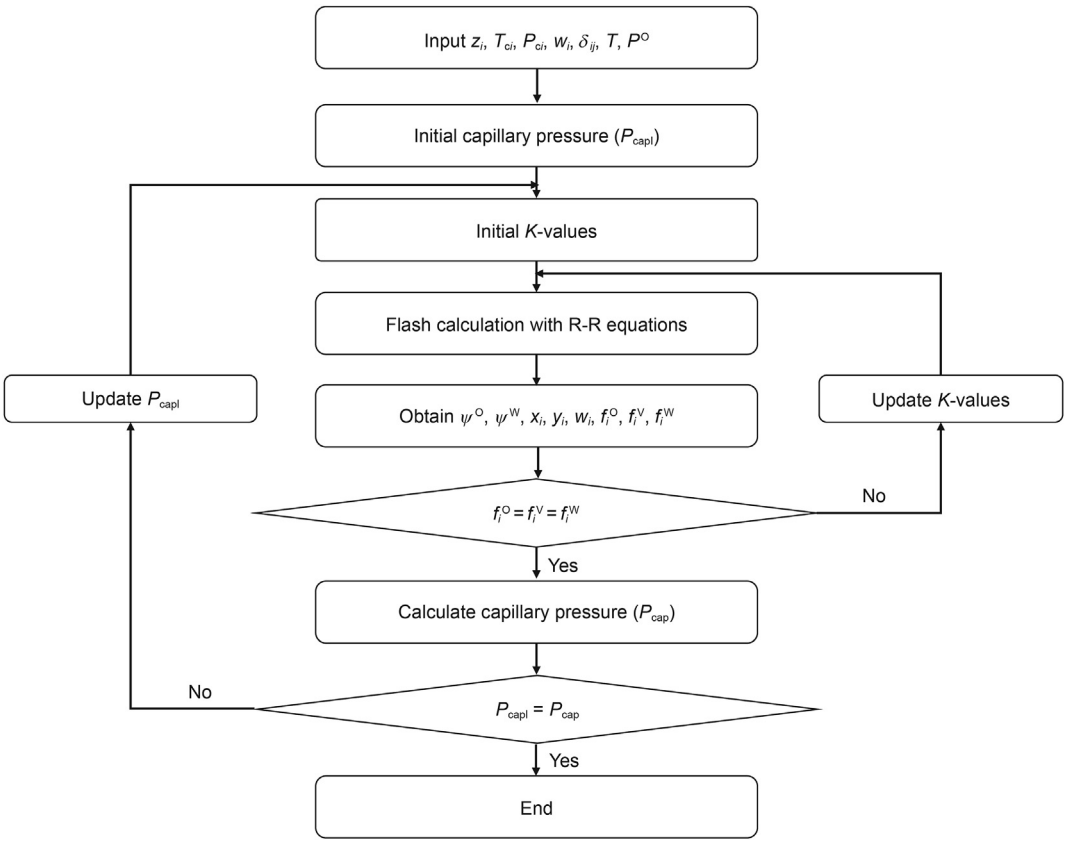

Fig. 1. The flowchart for the improved three-phase flash calculation algorithm.

reservoirs (Feng et al., 2018b).

A considerable amount of literature has been published on the nanopore confinement effect (Luo, 2018; Pitakbunkate et al., 2016; Zuo et al., 2018). Through laboratory experimental studies, it has been observed that the confinement leads to a reduction in the saturation pressure and critical property of confined fluids (Luo et al., 2019a; Tan et al., 2019). However, the experimental research mainly focuses on pure components and binary mixtures, and rarely involves mixtures above ternary (Salahshoor et al., 2018). In addition, laboratory experiments are difficult to truly reflect the unconventional characteristics of shale reservoirs, so the reliability of the experimental results remains to be discussed. To make up for the limitations of experimental research, molecular simulation methods have been applied to the study of the phase behavior of confined fluids (Feng et al., 2020; Liu and Zhang, 2019; Xiong et al., 2017). Molecular simulations can provide more information about the fluid phase behavior in small spaces (Wang et al., 2021; Wu et al., 2016). But the increase in pore size or fluid complexity requires more approximation and more computational time, so it is not suitable for complex mixtures and larger spaces (Song et al., 2021b). Few studies have used molecular simulation to analyze the fluid phase behavior in pores with a radius greater than 5 nm. Thus, the development of universal and easy-to-use equation of state (EOS) models to characterize the confined fluid phase behavior has attracted increasing attention.

Extensive research has been conducted to introduce capillary pressure and adsorption data into the traditional EOS and then to determine the phase equilibrium of fluids (Dong et al., 2016; Li and Sheng, 2017; Yan et al., 2017). However, the conventional EOS equation fails to describe confinement in nature. Hence, investigators have been working to form an EOS that can consider the confinement effect (Xiong et al., 2021b). Travalloni et al. (2010) presented an extended van der Waals EOS using two interaction parameters to study the adsorption behavior of confined fluids. Luo et al. (2019b) modified the Peng-Robinson EOS with a wall-molecule interaction coefficient to compute the phase transition pressure and temperature in nanopores. Araújo and Franco (2019) developed a new Statistical Associating Fluid Theory EOS to calculate the adsorption isotherms of confined mixtures. Zhang et al. (2019) extended the Soave-Redlich-Kwong EOS considering the fluid-pore wall interaction to calculate the critical pressure and temperature of confined fluids. Song et al. (2020b) proposed an adsorption-dependent EOS (A-PR-EOS) based on the description of fluid adsorption and discussed the effect of fluid adsorption on the critical property shifts. However, the existing research on the confinement effect mainly focuses on hydrocarbons, and there is little discussion about aqueous systems.

The shale oil reservoir contains considerable water in the form of water film or irreducible water (Feng et al., 2018a; Li et al., 2016b). Moreover, during stimulated reservoir volume (SRV) fracturing in a horizontal well tens of thousands of cubic meters of fracturing fluids (the main component is water) are injected into

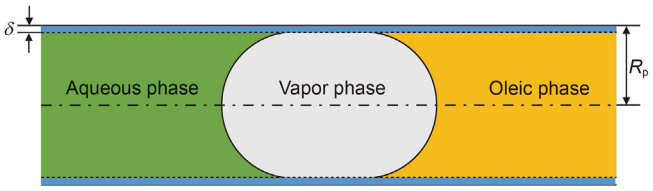

Fig. 2. A fluid distribution model considering adsorption and capillarity.

the formation, which increases the water saturation (Zhou et al., 2020). Several attempts have been made to study the phase behavior of the water-hydrocarbon-gas mixture in nanopores. Sun and Li (2019) presented a three-phase flash algorithm coupled with PR-EOS and capillary pressure to calculate the pressure-temperature envelope of the aqueous-oleic-vapor three-phase system. Xiong et al. (2021a) proposed an extended cubic-plus-association EOS to determine the interfacial tensions (IFT) of CH_4–CO_2–H_2O mixtures in shale nanopores. Zhao et al. (2021) calculated the IFT of H_2O–CO_2 and n-$C_{10}H_{22}$–CO_2 systems in nanopores based on an association EOS. However, these models do not consider the effect of water-oil-gas adsorption on the fluid phase behavior. Considering the coexistence of oil, gas and water, the adsorption and distribution of fluids in the matrix pores will make the mutual solubility and the fluid properties more complicated (Guo et al., 2019; Li et al., 2016a). It is necessary to develop a new thermodynamic model that is suitable for the water-oil-gas system and can reflect the confinement effect, including fluid adsorption and capillarity.

In this study, a novel three-phase flash algorithm considering the effect of nanopore confinement is developed to study the mutual solubility and fluid properties of water-oil-gas mixtures. A shale oil sample from Bakken is utilized in the case study. The effect of nanopore confinement on the phase mole fraction, phase equilibrium coefficient, phase density, and interfacial tension of the water-Bakken oil-CO_2 mixture is discussed in detail.

2. Modeling methodology

2.1. Improved three-phase flash algorithm

When the fugacity (f) of each component is equal in any phase, the three-phase equilibrium can be reached. For a multicomponent mixture, the fugacity-equality condition (Sun and Li, 2019) is given as,

$$f_i^{\mathrm{W}}\left(w,T,P^{\mathrm{W}}\right)=f_i^{\mathrm{O}}\left(x,T,P^{\mathrm{W}}\right)=f_i^{\mathrm{V}}\left(y,T,P^{\mathrm{W}}\right),\qquad i=1,\ldots,N_{\mathrm{c}} \tag{1}$$

where superscript W, O, and V represent the aqueous, oleic, and vapor phases, respectively; w, x, and y are the mole fractions of each component in the aqueous, oleic, and vapor phases, respectively; P is the pressure; T is the temperature; N_c is the component number in the mixture. It is noted that the fugacity of each component is affected by the adsorption effect, and the pressure in each phase is different due to the capillary pressure. These need to be considered in the judgment of fugacity-equality to improve the flash algorithm.

During the three-phase equilibrium calculations, distribution coefficients of components between the three phases are indispensable parameters.

$$\begin{cases} K_i^{\mathrm{W}}=\dfrac{y_i}{w_i} \\ K_i^{\mathrm{O}}=\dfrac{y_i}{x_i} \end{cases},\qquad i=1,\ldots,N_{\mathrm{c}} \tag{2}$$

where K_i^{W} and K_i^{O} are the vapor-aqueous equilibrium coefficient and vapor-oleic equilibrium coefficient of the ith component, respectively. Based on the material balance equations and the definition of phase equilibrium coefficient, the following objective equations (R-R equations) for a three-phase equilibrium can be obtained,

$$\begin{cases} \displaystyle\sum_{i=1}^{N_c} w_i-\sum_{i=1}^{N_c} y_i=\sum_{i=1}^{N_c}\frac{z_iK_i^{\mathrm{O}}\left(1-K_i^{\mathrm{W}}\right)}{K_i^{\mathrm{W}}K_i^{\mathrm{O}}+\psi^{\mathrm{W}}K_i^{\mathrm{O}}\left(1-K_i^{\mathrm{W}}\right)+\psi^{\mathrm{O}}K_i^{\mathrm{W}}\left(1-K_i^{\mathrm{O}}\right)}=0 \\ \displaystyle\sum_{i=1}^{N_c} x_i-\sum_{i=1}^{N_c} y_i=\sum_{i=1}^{N_c}\frac{z_iK_i^{\mathrm{W}}\left(1-K_i^{\mathrm{O}}\right)}{K_i^{\mathrm{W}}K_i^{\mathrm{O}}+\psi^{\mathrm{W}}K_i^{\mathrm{O}}\left(1-K_i^{\mathrm{W}}\right)+\psi^{\mathrm{O}}K_i^{\mathrm{W}}\left(1-K_i^{\mathrm{O}}\right)}=0 \end{cases},\qquad i=1,\ldots,N_{\mathrm{c}} \tag{3}$$

where z_i is the overall mole fraction of ith component; ψ^{W} and ψ^{O} are the mole fractions of the aqueous and oleic phases, respectively. If we know the phase equilibrium coefficients of each component, we can solve the R-R equations for ψ^{W}, ψ^{O}, x_i, y_i, and w_i.

A flowchart for the three-phase flash calculation procedure is provided in Fig. 1. The flowchart can be summarized as follows.

(1) Input the feed composition, component properties, temperature, oleic phase pressure, and initialize capillary pressure (P_{capl}).
(2) Initial phase equilibrium coefficient (K-values).
(3) Calculate ψ^{O}, ψ^{W}, x_i, y_i, w_i, f_i^{O}, f_i^{V}, f_i^{W} by flash calculation with R-R equations.
(4) If $f_i^{\mathrm{O}}=f_i^{\mathrm{V}}=f_i^{\mathrm{W}}$ is reached, then calculate capillary pressure. Otherwise, update K-values and repeat Steps 3 to 4. The K-values are updated by,

$$\begin{cases} K^{W}_{(n+1)} = \dfrac{f^{W}_{(n)}}{f^{V}_{(n)}} K^{W}_{(n)} \\ K^{O}_{(n+1)} = \dfrac{f^{O}_{(n)}}{f^{V}_{(n)}} K^{O}_{(n)} \end{cases} \tag{4}$$

(5) IF the calculated capillary pressure is equal to the initial capillary pressure, the calculation ends. Otherwise, update initial capillary pressure ($P_{capI} = P_{cap}$) and repeat Steps 2 to 5.

In the following sections, the calculation methods of the fugacity and capillary pressure are discussed in detail.

2.2. Fugacity calculation considering fluid adsorption

A fugacity calculation method for oil-gas mixtures has been proposed to consider the adsorption effect using A-PR-EOS in a previous study (Song et al., 2020b). In this paper, based on the A-PR-EOS and the description of water-oil-gas adsorption, a new formula is developed to determine the fugacity in water-oil-gas systems, the details of the fugacity calculation formula derivation are listed in the *Supplementary Information*.

$$\ln\frac{f_i}{c_i P} = \frac{B_i}{B}(Z-1) - \ln(Z-B) - \frac{A}{2\sqrt{2}B}\left[\frac{2\sum_{j=1}^{N_c}(A_iA_j)^{0.5}(1-k_{ij})}{A} - \frac{B_i}{B}\right]\ln\left[\frac{Z+B\left(1+\sqrt{2}\right)}{Z+B\left(1-\sqrt{2}\right)}\right], \quad i,j=1,\ldots,N_c \tag{5}$$

where c_i and c_j are the mole fraction of the ith and jth components in any phase, respectively; Z is the compressibility factor; k_{ij} is the binary interaction parameter (BIP); A and B are the EOS parameter.

$$\begin{cases} A = \sum_{i=1}^{N_c}\sum_{j=1}^{N_c} c_i c_j (A_iA_j)^{0.5}(1-k_{ij}) \\ B = \sum_{i=1}^{N_c} c_i B_i \end{cases}, \quad i,j=1,\ldots,N_c \tag{6}$$

and,

$$\begin{cases} A_i = 0.45724\dfrac{R^2T_{ci}^2}{P_{ci}}\left[1+\left(0.37464+1.54226\omega-0.26992\omega^2\right)\left(1-\sqrt{\dfrac{T}{T_{ci}}}\right)\right]^2 \\ B_i = 0.07780\dfrac{RT_{ci}}{P_{ci}}(1-\gamma\beta) \\ \gamma = \dfrac{2\delta}{R_p} - \left(\dfrac{\delta}{R_p}\right)^2 \end{cases}, \quad i=1,\ldots,N_c \tag{7}$$

where P_{ci} is the critical pressure of the ith component; T_{ci} is the critical temperature of the ith component; R is the universal gas constant; β is the reduced adsorption density; γ is the dimensionless adsorption radius; R_p is the pore radius; δ is the adsorption thickness.

As for the oil-gas system, the reduced adsorption density β_{og} and the adsorption thickness δ_{og} can be calculated by,

$$\begin{cases} \beta_{og} = \sum_{i=1}^{N_c} z_i\beta_i \\ \delta_{og} = \sum_{i=1}^{N_c} z_i\delta_i \end{cases}, \quad i=1,\ldots,N_c \tag{8}$$

and,

$$\begin{cases} \beta_i = 0.6794\dfrac{(\sigma_{LJ}/R_p)^{0.7878}}{2\delta/R_p - (\delta/R_p)^2} \\ \delta_i = \dfrac{m}{\ln(R_p/\sigma_{LJ})} + n\left(\dfrac{\sigma_{LJ}}{R_p}\right) \end{cases} \tag{9}$$

where m and n are empirical parameters; σ_{LJ} is the Lennard-Jones size parameter.

As for the water system, the reduced adsorption density β_w and the adsorption thickness δ_w can be calculated by,

$$\begin{cases} \beta_w = -3.3081(\sigma_{LJ}/R_p)^3 + 0.1622(\sigma_{LJ}/R_p)^2 + 0.6280(\sigma_{LJ}/R_p) + 1.1170 \\ \delta_w = -0.7022(\sigma_{LJ}/R_p)^2 + 0.3964(\sigma_{LJ}/R_p) + 0.6131 \end{cases} \tag{10}$$

As for the water-oil-gas mixture, the reduced adsorption density β and the adsorption thickness δ can be calculated by,

$$\begin{cases} \beta = (1-\varepsilon)\beta_{og} + \varepsilon\beta_w \\ \delta = (1-\varepsilon)\delta_{og} + \varepsilon\delta_w \end{cases} \tag{11}$$

where ε represents the coverage coefficient of water, which is the fraction of the wetted area of water molecules in the total pore area. In this study, ε is approximately set equal to the water feed.

2.3. Capillary pressure calculation

According to the research of many scholars, the fluid distribution of a three-phase system is very complicated in a confined space, which causes the diversity of the capillary pressure in shale nanopores. Sun and Li (2019) summarized six possible fluid distributions considering capillary pressure, and their research showed that for different fluid distributions, capillary pressure has similar effects on phase behavior. Thus, in this work, we only choose one possible fluid distribution to study the effect of capillarity. The given fluid distribution model considering adsorption and capillarity in a 1D capillary tube is proposed, as shown in Fig. 2.

Table 1
Composition data of the water-oil-CO_2 mixture (Nojabaei et al., 2013).

Component	z_i	P_c, KPa	T_c, K	M_W, lb/mol	ω	Parachor
H_2O	1.00000	22088.85	647.30	18.015	0.3440	52.0
CO_2	1.00000	7376.46	304.20	44.010	0.2250	78.0
C_1	0.36736	4516.20	186.30	16.535	0.0102	74.8
C_2	0.14885	4977.94	305.54	30.433	0.1028	107.7
C_3	0.09334	4245.51	369.98	44.097	0.1520	151.9
C_4	0.05751	3767.71	421.78	58.124	0.1894	189.6
C_5–C_6	0.06404	3180.48	486.38	78.295	0.2684	250.2
C_7–C_{12}	0.15854	2505.14	585.14	120.562	0.4291	350.2
C_{13}–C_{21}	0.0733	1721.00	740.05	220.716	0.7203	590.0
C_{22}–C_{80}	0.03704	1310.83	1024.72	443.518	1.0159	1216.8

As for the fluid distribution shown in the Fig. 2, the relationship of the three phase pressures can be expressed as,

$$\begin{cases} P^V - P^W = P_{cvw} \\ P^V - P^O = P_{cvo} \end{cases} \tag{12}$$

where P_{cvw} is the capillary pressure between the vapor and aqueous phases; P_{cvo} is the capillary pressure between the vapor and oleic phases.

The Young-Laplace equation is served as the basic model to calculate the capillary pressure. With the modified pore radius and interfacial tension (IFT) (Tan and Piri, 2015) and the assumptions of zero contact angle, the traditional Yong-Laplace is modified to calculate P_{cvw} and P_{cvo}.

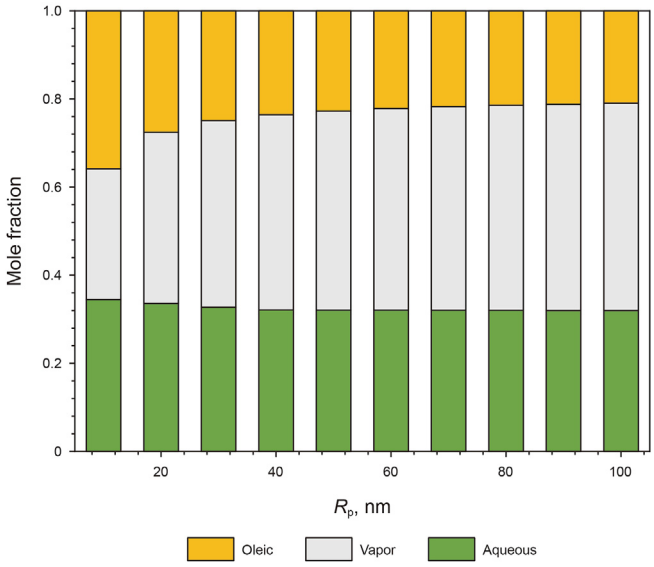

Fig. 3. The phase mole fraction of the water-oil-CO_2 mixture at $P = 10$ MPa and $T = 388.7$ K.

Table 2
BIPs of the water-oil-CO_2 mixture (Nojabaei et al., 2013).

Component	H_2O	CO_2	C_1	C_2	C_3	C_4	C_5–C_6	C_7–C_{12}	C_{13}–C_{21}	C_{22}–C_{80}
H_2O	0	0.0952	0.4500	0.4500	0.5300	0.5200	0.5200	0.5000	0.5000	0.5000
CO_2	0.0952	0	0.1200	0.1200	0.1200	0.1200	0.1200	0.1200	0.1200	0.1200
C_1	0.4500	0.1200	0	0.0050	0.0035	0.0035	0.0037	0.0033	0.0033	0.0033
C_2	0.4500	0.1200	0.0050	0	0.0031	0.0031	0.0031	0.0026	0.0026	0.0026
C_3	0.5300	0.1200	0.0035	0.0031	0	0	0	0	0	0
C_4	0.5200	0.1200	0.0035	0.0031	0	0	0	0	0	0
C_5–C_6	0.5200	0.1200	0.0037	0.0031	0	0	0	0	0	0
C_7–C_{12}	0.5000	0.1200	0.0033	0.0026	0	0	0	0	0	0
C_{13}–C_{21}	0.5000	0.1200	0.0033	0.0026	0	0	0	0	0	0
C_{22}–C_{80}	0.5000	0.1200	0.0033	0.0026	0	0	0	0	0	0

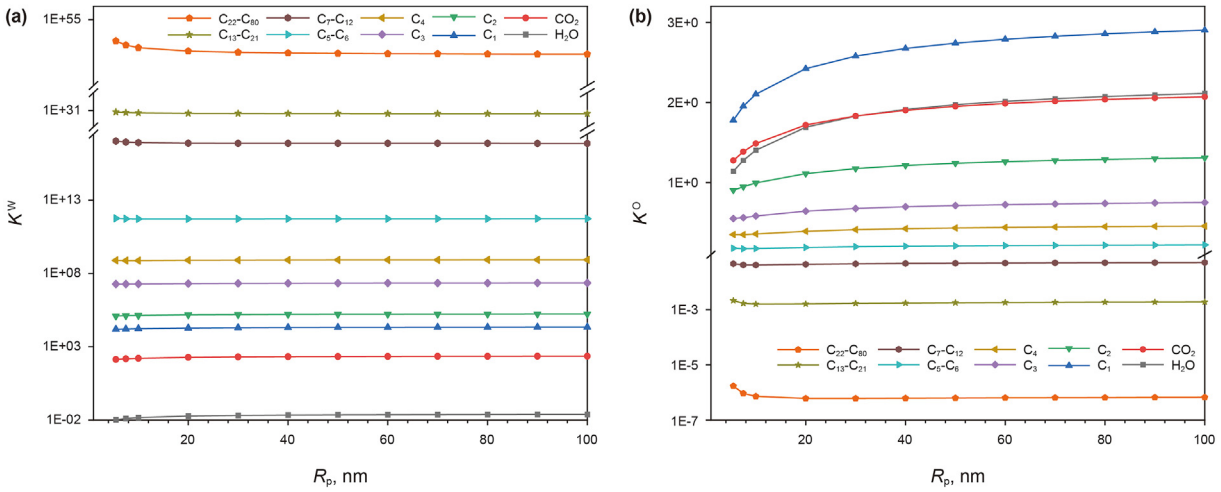

Fig. 4. The phase equilibrium coefficient of the water-oil-CO_2 mixture at $P = 10$ MPa and $T = 388.7$ K: (**a**) vapor-aqueous equilibrium coefficient; (**b**) vapor-oleic equilibrium coefficient.

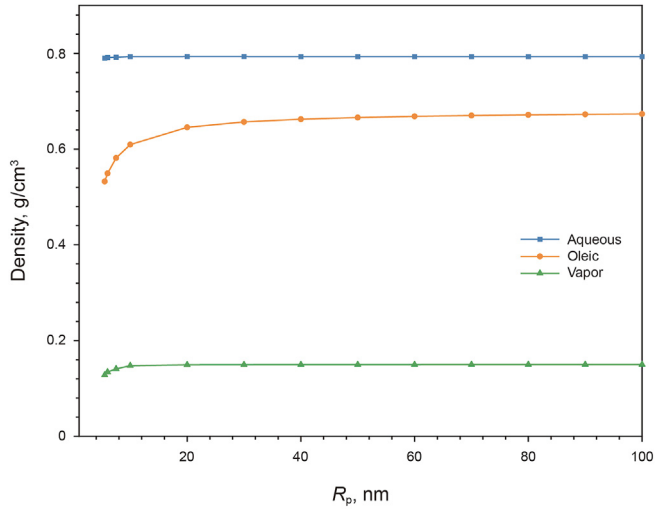

Fig. 5. The phase density of the water-oil-CO_2 mixture at $P = 10$ MPa and $T = 388.7$ K.

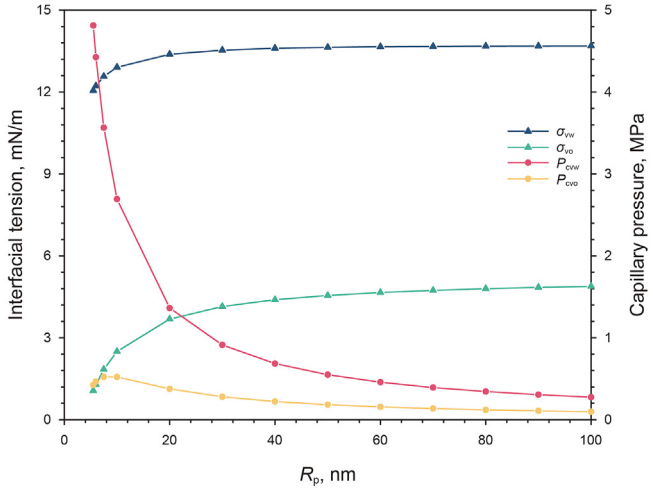

Fig. 6. The interfacial tension and capillary pressure of the water-oil-CO_2 mixture at $P = 10$ MPa and $T = 388.7$ K.

$$\begin{cases} P_{\mathrm{cvw}} = \dfrac{2\sigma_{\mathrm{vw}}}{R_{\mathrm{p}} - \delta} \\ P_{\mathrm{cvo}} = \dfrac{2\sigma_{\mathrm{vo}}}{R_{\mathrm{p}} - \delta} \end{cases} \tag{13}$$

and

$$\begin{cases} \sigma_{\mathrm{vw}} = \dfrac{\sigma_{\mathrm{vw}}^{\infty}}{1 + 2\dfrac{\delta}{R_{\mathrm{p}} - \delta}} \\ \sigma_{\mathrm{vo}} = \dfrac{\sigma_{\mathrm{vo}}^{\infty}}{1 + 2\dfrac{\delta}{R_{\mathrm{p}} - \delta}} \end{cases} \tag{14}$$

where σ_{vw} is the IFT between vapor and aqueous phases in nanopore; σ_{vo} is the IFT between vapor and oleic phases in nanopore; $\sigma_{\mathrm{vw}}^{\infty}$ is the flat surface tension between vapor and aqueous phases; $\sigma_{\mathrm{vo}}^{\infty}$ is the flat surface tension between vapor and oleic phases.

The Macled-Sugden equation (Weinaug and Katz, 1943) has been widely used to predict the interaction tension of oleic-vapor and aqueous-vapor (Dong et al., 2016; Sun and Li, 2019). Therefore, The Macleod-Sugden equation is chosen to calculate the flat surface tension between two phases in this paper,

$$\begin{cases} \sigma_{\mathrm{vw}}^{\infty} = \left[\sum_{i=1}^{N_{\mathrm{c}}} P_{\mathrm{ch}i}\left(w_i\rho^{\mathrm{W}} - y_i\rho^{\mathrm{V}}\right)\right]^4 \\ \sigma_{\mathrm{vo}}^{\infty} = \left[\sum_{i=1}^{N_{\mathrm{c}}} P_{\mathrm{ch}i}\left(x_i\rho^{\mathrm{O}} - y_i\rho^{\mathrm{V}}\right)\right]^4 \end{cases}, \quad i = 1, \ldots, N_{\mathrm{c}} \tag{15}$$

where $P_{\mathrm{ch}i}$ is the parachor; ρ^{W}, ρ^{O} and ρ^{V} are the molar density of the aqueous, oleic, and vapor phases, respectively.

3. Results and discussion

The effect of confinement on the three-phase equilibrium of the water-oil-CO_2 mixture is discussed. A shale oil sample from the Bakken reservoir (Nojabaei et al., 2013) is utilized in the case study.

The physical properties and the BIPs of the components are shown in Tables 1 and 2, respectively. The phase equilibrium coefficients of the water-oil-gas mixture in the bulk state are calculated and compared with the PVTsim software and with our three-phase flash code, and the comparison results are shown in Table S3 in the *Supplementary Information*. It is found that the phase equilibrium coefficients calculated by our code are very consistent with those calculated from PVTsim (The average error is 0.023%), which verifies the correctness and robustness of our algorithm.

3.1. Phase mole fraction

The effect of confinement on the mass transport of water-oil-gas mixtures is investigated using the improved three-phase flash algorithm. Fig. 3 shows the phase mole fractions of the water-oil-CO_2 mixture under different pore radii at $P = 10$ MPa and $T = 388.7$ K. The system contains 32.02 mol% aqueous, 20.99 mol% oleic, and 46.99 mol% vapor under the pore radius of 100 nm. With a decrease in the pore size (especially when the R_p is less than 40 nm), the mole fraction of the vapor phase decreases, and the mole fraction of oleic and aqueous phases increases. When the pore radius is reduced to 10 nm, the mole fraction of the aqueous phase slightly increases to 34.46%, the mole fraction of the oleic phase increases to 35.82%, and the mole fraction of the vapor phase decreases to 29.72%. The result shows that the nanopore confinement effect promotes the transfer of molecules in the vapor phase to the aqueous and oleic phases. That is because the confined molecules have a layered and ordered structure caused by the nanopore constraints and the fluid-wall interactions (Wu et al., 2016). Therefore, the molecules in nanopores have a tendency to form denser phases, namely the aqueous and oleic phases.

3.2. Phase equilibrium coefficient

In this section, the phase equilibrium coefficients of the water-oil-CO_2 mixture are calculated to further illustrate the effect of confinement on mass transport. Fig. 4 presents the vapor-aqueous equilibrium coefficient (K^W) and vapor-oleic equilibrium coefficient (K^O) of each component under different pore radii. As the pore size decreases, the K^W and K^O of water, CO_2, and lighter hydrocarbons (including C_1, C_2, C_3, and C_4) are all decreased, the K^W and K^O of heavier hydrocarbon (including C_5–C_6, C_7–C_{12}, C_{12}–C_{21}, and C_{22}–C_{28}) are all increased. This means that all components in the vapor phase tend to enter the other phases, but the transfer of water, CO_2, and lighter hydrocarbons is more significant due to their high initial content in the vapor phase. An important phenomenon can also be found in Fig. 4: for almost all components, the change of K^O is more significant than K^W. In other words, the confinement effect presents a greater impact on the transfers between the vapor and oleic phases than the component between the vapor and aqueous phases.

3.3. Phase density

Here, the fluid phase density of the water-oil-CO_2 mixture under different pore sizes is calculated and shown in Fig. 5. The result shows that the density of the aqueous phase is almost unchanged, the density of the oleic phase is reduced sharply, the density of the vapor phase is reduced slightly with the reduction of pore radius. That causes the density difference between the aqueous and vapor phases to increase and the density difference between the oleic and vapor phases to decrease. The reason is that the heavy components have a greater tendency to enter the oleic phase than light components (Song et al., 2020a), resulting in an increase in the proportion of light components in the vapor phase and a slight decrease in the density of the vapor phase. On the other hand, due to the high initial content of light components in the vapor phase, the number of light components entering the oleic phase is greater than the number of heavy components. Therefore, the light components in the oleic phase increase, and the density of the oleic phase decreases.

3.4. Interfacial tension and capillary pressure

Fig. 6 shows the IFT of the water-oil-CO_2 mixture under different pore radius. It can be observed that the IFT between vapor and aqueous phases (σ_{vw}) and the IFT between vapor and oleic phases (σ_{vo}) are both decreased with the reduction of the pore size. Due to the presence of nanopore confinement, the composition differences between vapor and liquid phases become smaller, leading to a decrease in σ_{vw} and σ_{vo}. Besides, the confinement effect presents a greater impact on the transfers between the vapor and oleic phases than the transfers between the vapor and aqueous phases. Thus, the change of σ_{vo} is more significant than σ_{vw}, as shown in Fig. 6.

The capillary pressures of the water-oil-CO_2 mixture under different pore radii are also shown in Fig. 6. As the pore size becomes smaller, the capillary pressure between vapor and aqueous phases (P_{cvw}) continues to increase; however, the capillary pressure between vapor and oleic phases (P_{cvo}) increases under larger pore sizes and then decreases under extremely small pore sizes (such as $R_p < 7$ nm). It can be attributed to the fact that the reduced IFT and the decreased pore size have opposite effects on capillary pressure. For the vapor-aqueous phases, the σ_{vw} changes slowly, so the influence of the pore radius is dominant. For the vapor-oleic phases, the σ_{vo} changes slowly under a larger pore radius, thus the influence of pore radius is also dominant; However, the σ_{vo} changes greatly under extremely small pore radii, thus the σ_{vo} is relatively more dominant in P_{cvo}, resulting in a decrease in P_{cvo} as the pore size decreases.

4. Conclusions

In this study, an improved three-phase flash algorithm is proposed to study the effect of nanopore confinement, i.e., the synthetic effect of fluid adsorption and capillary pressure on the phase equilibrium of the water-oil-CO_2 mixture. The main finding and conclusions are summarized as follows.

(1) The confinement effect promotes the transfer of components in the vapor phase to the aqueous and oleic phases, and the transfer of water, CO_2, and lighter hydrocarbons is more significant. This leads to a large decrease, a large increase, and a small increase in the mole fractions of the vapor, oleic, and aqueous phases, respectively.
(2) Due to the confinement effect, the density difference between the aqueous and vapor phases increases, and the density difference between the oleic and vapor phases decreases.
(3) When the confinement effect is considered, the σ_{vw} and σ_{vo} are both decreased with the reduction of the pore size, while the change of σ_{vo} is more significant than σ_{vw}.
(4) The P_{cvw} continues to increase with the reduction of the pore size; however, the P_{cvo} increases under larger pore size and then decreases under smaller pore size (such as $R_p < 7$ nm).
(5) The confinement effect presents a greater impact on the transfers between the vapor and oleic phases than the transfers between the vapor and aqueous phases. Besides,

when the R_p is less than 40 nm, the confinement effect is noteworthy and cannot be ignored.

Declaration of competing interest

The authors declare no competing financial interest.

Acknowledgements

The financial support from National Natural Science Foundation of China (52074319, U19B6003-02) and Strategic Cooperation Technology Project of CNPC (ZLZX 2020-01-08) is gratefully acknowledged. We also wish to thank Haining Zhao at China University of Petroleum-Beijing for his great help on the phase behavior calculation.

Appendix A. Supplementary data

Supplementary data to this article can be found online at https://doi.org/10.1016/j.petsci.2021.09.024.

References

Araújo, I.S., Franco, L.F.M., 2019. A model to predict adsorption of mixtures coupled with SAFT-VR Mie Equation of state. Fluid Phase Equil. 496, 61–68. https://doi.org/10.1016/j.fluid.2019.05.021.

Dong, X., Liu, H., Hou, J., Wu, K., Chen, Z., 2016. Phase equilibria of confined fluids in nanopores of tight and shale rocks considering the effect of capillary pressure and adsorption film. Ind. Eng. Chem. Res. 55 (3), 798–811. https://doi.org/10.1021/acs.iecr.5b04276.

Feng, D., Li, X., Wang, X., Li, J., Sun, F., Sun, Z., Zhang, T., Li, P., Chen, Y., Zhang, X., 2018a. Water adsorption and its impact on the pore structure characteristics of shale clay. Appl. Clay Sci. 155, 126–138. https://doi.org/10.1016/j.clay.2018.01.017.

Feng, D., Li, X., Wang, X., Li, J., Zhang, X., 2018b. Capillary filling under nanoconfinement: the relationship between effective viscosity and water-wall interactions. Int. J. Heat Mass Tran. 118, 900–910. https://doi.org/10.1016/j.ijheatmasstransfer.2017.11.049.

Feng, Q., Xu, S., Xing, I., Zhang, W., Wang, S., 2020. Advances and challenges in shale oil development: a critical review. Advances in Geo-Energy Research 4 (4), 406–418. https://doi.org/10.46690/ager.2020.04.06.

Feng, D., Bakhshian, S., Wu, K., Song, Z., Ren, B., Li, J., Hosseini, S.A., Li, X., 2021. Wettability effects on phase behavior and interfacial tension in shale nanopores. Fuel 290, 119983. https://doi.org/10.1016/j.fuel.2020.119983.

Guo, C., Liu, H., Xu, L., Zhou, Q., 2019. An improved transport model of shale gas considering three-phase adsorption mechanism in nanopores. J. Petrol. Sci. Eng. 182, 106291. https://doi.org/10.1016/j.petrol.2019.106291.

Li, J., Li, X., Wang, X., Li, Y., Wu, K., Shi, J., Yang, L., Feng, D., Zhang, T., Yu, P., 2016a. Water distribution characteristic and effect on methane adsorption capacity in shale clay. Int. J. Coal Geol. 159, 135–154. https://doi.org/10.1016/j.coal.2016.03.012.

Li, J., Li, X., Wu, K., Wang, X., Shi, J., Yang, L., Zhang, H., Sun, Z., Wang, R., Feng, D., 2016b. Water sorption and distribution characteristics in clay and shale: effect of surface force. Energy Fuel. 30 (11), 8863–8874. https://doi.org/10.1021/acs.energyfuels.6b00927.

Li, L., Sheng, J.J., 2017. Nanopore confinement effects on phase behavior and capillary pressure in a Wolfcamp shale reservoir. Journal of the Taiwan Institute of Chemical Engineers 78, 317–328. https://doi.org/10.1016/j.jtice.2017.06.024.

Liu, X., Zhang, D., 2019. A review of phase behavior simulation of hydrocarbons in confined space: implications for shale oil and shale gas. J. Nat. Gas Sci. Eng. 68, 102901. https://doi.org/10.1016/j.jngse.2019.102901.

Liu, Y., Li, H.A., Okuno, R., 2018. Phase behavior of N_2/n-C_4H_{10} in a partially confined space derived from shale sample. J. Petrol. Sci. Eng. 160, 442–451. https://doi.org/10.1016/j.petrol.2017.10.061.

Luo, S., 2018. Confinement affects phase behavior of petroleum fluids in shale reservoirs. In: SPE Annual Technical Conference and Exhibition. https://doi.org/10.2118/194041-STU.

Luo, S., Lutkenhaus, J.L., Nasrabadi, H., 2019a. Experimental study of pore size distribution effect on phase transitions of hydrocarbons in nanoporous media. Fluid Phase Equil. 487, 8–15. https://doi.org/10.1016/j.fluid.2018.11.026.

Luo, S., Jin, B., Lutkenhaus, J.L., Nasrabadi, H., 2019b. A novel pore-size-dependent equation of state for modeling fluid phase behavior in nanopores. Fluid Phase Equil. 498, 72–85. https://doi.org/10.1016/j.fluid.2019.06.009.

Nojabaei, B., Johns, R.T., Chu, L., 2013. Effect of capillary pressure on phase behavior in tight rocks and shales. SPE Reservoir Eval. Eng. 16 (3), 281–289. https://doi.org/10.2118/159258-PA.

Pitakbunkate, T., Balbuena, P.B., Moridis, G.J., Blasingame, T.A., 2016. Effect of confinement on pressure/volume/temperature properties of hydrocarbons in shale reservoirs. SPE J. 21 (2), 621–634. https://doi.org/10.2118/170685-PA.

Salahshoor, S., Fahes, M., Teodoriu, C., 2018. A review on the effect of confinement on phase behavior in tight formations. J. Nat. Gas Sci. Eng. 51, 89–103. https://doi.org/10.1016/j.jngse.2017.12.011.

Song, Y., Song, Z., Feng, D., Qin, J., Chen, Y., Shi, Y., Hou, J., Song, K., 2020a. Phase behavior of hydrocarbon mixture in shale nanopores considering the effect of adsorption and its induced critical shifts. Ind. Eng. Chem. Res. 59 (17), 8374–8382. https://doi.org/10.1021/acs.iecr.0c00490.

Song, Z., Song, Y., Guo, J., Zhang, Z., Hou, J., 2020b. Adsorption induced critical shifts of confined fluids in shale nanopores. Chem. Eng. J. 385, 123837. https://doi.org/10.1016/j.cej.2019.123837.

Song, Y., Song, Z., Guo, J., Feng, D., Chang, X., 2021a. Phase behavior and miscibility of CO_2-hydrocarbon mixtures in shale nanopores. Ind. Eng. Chem. Res. 60, 1463–1472. https://doi.org/10.1021/acs.iecr.1c00717.

Song, Z., Song, Y., Guo, J., Feng, D., Dong, J., 2021b. Effect of nanopore confinement on fluid phase behavior and production performance in shale oil reservoir. Ind. Eng. Chem. Res. 60, 5300–5309. https://doi.org/10.1021/acs.iecr.0c05814.

Song, Z., Song, Y., Li, Y., Bai, B., Song, K., Hou, J., 2020c. A critical review of CO_2 enhanced oil recovery in tight oil reservoirs of North America and China. Fuel 276, 118006. https://doi.org/10.1016/j.fuel.2020.118006.

Sun, H., Li, H.A., 2019. A new three-phase flash algorithm considering capillary pressure in a confined space. Chem. Eng. Sci. 193, 346–363. https://doi.org/10.1016/j.ces.2018.09.013.

Tan, S.P., Piri, M., 2015. Equation-of-state modeling of confined-fluid phase equilibria in nanopores. Fluid Phase Equil. 393, 48–63. https://doi.org/10.1016/j.fluid.2015.02.028.

Tan, S.P., Qiu, X., Dejam, M., Adidharma, H., 2019. Critical point of fluid confined in nanopores: experimental detection and measurement. J. Phys. Chem. C 123 (15), 9824–9830. https://doi.org/10.1021/acs.jpcc.9b00299.

Travalloni, L., Castier, M., Tavares, F.W., Sandler, S.I., 2010. Thermodynamic modeling of confined fluids using an extension of the generalized van der Waals theory. Chem. Eng. Sci. 65 (10), 3088–3099. https://doi.org/10.1016/j.ces.2010.01.032.

Wang, S., Yao, X., Feng, Q., Javadpour, F., Yang, Y., Xue, Q., Li, X., 2021. Molecular insights into carbon dioxide enhanced multi-component shale gas recovery and its sequestration in realistic kerogen. Chem. Eng. J. 425, 130292. https://doi.org/10.1016/j.cej.2021.130292.

Weinaug, C., Katz, D., 1943. Surface tensions of methane-propane mixtures. Ind. Eng. Chem. 35 (2), 239–246. https://doi.org/10.1021/ie50398a028.

Wu, K., Chen, Z., Li, X., Dong, X., 2016. Methane storage in nanoporous material at supercritical temperature over a wide range of pressures. Sci. Rep. 6 (1). https://doi.org/10.1038/srep33461.

Wu, S., Li, Z., Sarma, H.K., 2020. Influence of confinement effect on recovery mechanisms of CO_2-enhanced tight-oil recovery process considering critical properties shift, capillarity and adsorption. Fuel 262, 116569. https://doi.org/10.1016/j.fuel.2019.116569.

Xiong, J., Liu, X., Liang, L., Zeng, Q., 2017. Investigation of methane adsorption on chlorite by grand canonical Monte Carlo simulations. Petrol. Sci. 14 (1), 37–49. https://doi.org/10.1007/s12182-016-0142-1.

Xiong, W., Zhang, L., Zhao, Y., Wu, J., Huang, J., Yao, J., 2021a. A generalized equation of state for associating fluids in nanopores: application to CO_2-H_2O, CH_4-H_2O, CO_2-CH_4, and CO_2-CH_4-H_2O systems and implication for extracting dissolved CH_4 by CO_2 injection. Chem. Eng. Sci. 229, 116034. https://doi.org/10.1016/j.ces.2020.116034.

Xiong, W., Zhao, Y., Qin, J., Huang, S., Zhang, L., 2021b. Phase equilibrium modeling for confined fluids in nanopores using an association equation of state. J. Supercrit. Fluids 169, 105118. https://doi.org/10.1016/j.supflu.2020.105118.

Yan, B., Wang, Y., Killough, J.E., 2017. A fully compositional model considering the effect of nanopores in tight oil reservoirs. J. Petrol. Sci. Eng. 152, 675–682. https://doi.org/10.1016/j.petrol.2017.01.005.

Yang, G., Fan, Z., Li, X., 2019. Determination of confined fluid phase behavior using extended Peng-Robinson equation of state. Chem. Eng. J. 378, 122032. https://doi.org/10.1016/j.cej.2019.122032.

Zhang, K., Jia, N., Liu, L., 2019. Generalized critical shifts of confined fluids in nanopores with adsorptions. Chem. Eng. J. 372, 809–814. https://doi.org/10.1016/j.cej.2019.04.198.

Zhang, Y., Lashgari, H.R., Di, Y., Sepehrnoori, K., 2017. Capillary pressure effect on phase behavior of CO_2/hydrocarbons in unconventional reservoirs. Fuel 197, 575–582. https://doi.org/10.1016/j.fuel.2017.02.021.

Zhao, Y., Xiong, W., Zhang, L., Qin, J., Huang, S., Guo, J., He, X., Wu, J., 2021. Phase equilibrium modeling for interfacial tension of confined fluids in nanopores using an association equation of state. J. Supercrit. Fluids 176, 105322. https://doi.org/10.1016/j.supflu.2021.105322.

Zhou, W., Wang, H., Yang, X., Liu, X., Yan, Y., 2020. Confinement effects and CO_2/CH_4 competitive adsorption in realistic shale kerogen nanopores. Ind. Eng. Chem. Res. 59 (14), 6696–6706. https://doi.org/10.1021/acs.iecr.9b06549.

Zhu, C., Guo, W., Wang, Y., Li, Y., Gong, H., Xu, L., Dong, M., 2021. Experimental study of enhanced oil recovery by CO_2 huff-n-puff in shales and tight sandstones with fractures. Petrol. Sci. 18, 852–869. https://doi.org/10.1007/s12182-020-00538-7.

Zuo, J.Y., Guo, X., Liu, Y., Pan, S., Canas, J., Mullins, O.C., 2018. Impact of capillary pressure and nanopore confinement on phase behaviors of shale gas and oil. Energy Fuel. 32 (4), 4705–4714. https://doi.org/10.1021/acs.energyfuels.7b03975.